Fachtagung "Experimentelle Strömungsmechanik"
6. – 8. September 2016, Cottbus

Geschwindigkeitsmessung in einem axial geschichteten Taylor-Couette Experiment

PIV measurements in an axially stratified Taylor-Couette experiment

Torsten Seelig, Martin Burchardt, Andreas Krebs, Uwe Harlander, Christoph Egbers
Department of Aerodynamics and Fluid Mechanics
Brandenburg University of Technology (BTU) Cottbus - Senftenberg
Lehrgebäude 3A, Siemens-Halske-Ring 14
D-03046 Cottbus, Germany
Phone: +49-(0)355-69-3686
Fax: +49-(0)355-69-4891

PIV, Schichtung, Taylor-Couette
PIV, stratification, Taylor-Couette

Abstract

Context: Stratorotational instability (SRI) has been proposed as a mechanism for outward angular momentum transport in Keplerian accretion disks. A particular designed Taylor-Couette laboratory experiment with axial stratification is suitable for studying the instability. The bottom end-plate is cooled from below and the top end-plate is heated from above to achieve axial stratification. Due to constructive constraints, the end-plates are visually unamenable and quantitative measurement techniques in the co-rotating frame can only be done by looking through the outer cylinder. For this purpose we built a co-rotating mini-PIV (Particle Image Velocimetry) system with cameras having tilted viewing angles regarding the laser sheets.
Aims: To quantify the accuracy of mini-PIV and the novel calibration technique.
Methods: We perform measurements of the azimuthal and radial component of the velocity in axially stratified stable flows. We compare the time-averaged azimuthal velocity with the axially invariant Taylor-Couette solution.
Results: We show for the first time the significant reduction of global endwall effects in a linear stratified Taylor-Couette flow. We identify the absolute error to be 2% and the relative error to be 5.58% ± 0.052%.
Conclusion: The PIV technique together with the applied novel calibration technique is suitable to quantify SRI.

Introduction

Outward angular momentum transport in accretion disks is still an open question. The formation of planets in accretion disks cannot be understood without outward transport. Since without it the angular velocity of a nascent planet would be far to high. Only an instability, like waves or turbulence, can achieve such an outward angular momentum transport. For disks coupled with a magnetic field the Magneto Rotational Instability (MRI) occurs and, regardless of other angular momentum transport processes, one expects the fluid to sustain Magneto Hydrodynamic Turbulence. However, accretion disks can be unstable or turbulent even in the absence of a magnetic field, e.g. in regions where the ionization fraction is low. Within the last decade, among other candidates the SRI has attracted attention (Shalybkov and Rüdiger. 2005).

Karlsruhe, Germany, ISBN 978-3-9816764-2-6

The SRI is a purely hydrodynamic instability and much insight can be obtained from particularly designed laboratory experiments and numerical simulations in an axially-stratified Taylor-Couette setup (Le Bars and Le Gal. 2007, Gellert and Rüdiger. 2009, Rüdiger et al. 2013). Axial stratification is achieved either due to stratified saltwater (Thorpe 1966, Withjack and Chen. 1974, Boubnov et al. 1995, Le Bars and Le Gal. 2007) or due to cooling the lower and heating the upper lid (Gellert and Rüdiger. 2009). The temperature stratification represents the axial stratification of an accretion disk centered around a hot star where the rotation of the cylinders mimics the astrophysical rotation laws with rotation rate decreasing outwards.

The axially invariant solution of the angular velocity for classical Taylor-Couette flows is $\Omega(r) = a + b/r^2$. The two free constants (a,b) are fixed by Ω_{in} and Ω_{out}, the angular velocity of the inner cylinder (radius r_{in}) and the outer cylinder (radius r_{out}). It follows that $a = \Omega_{in}(\mu-\eta^2)/(1-\eta^2)$ and $b = r_{in}^2\Omega_{in}(1-\mu)/(1-\eta^2)$, being $\mu = \Omega_{out}/\Omega_{in}$ the rotation ratio and $\eta = r_{in}/r_{out}$ the radius ratio. The term b/r^2 is curl free and the profile is called potential flow. With respect to the theory of the Taylor-Couette flows it defines the Rayleigh limit. The potential flow at the Rayleigh limit is defined by $a = 0$, i.e. $\mu = \eta^2$ and separates the region of unstable flow from stable flow.

Thorpe (1966) performed the first experiments with stratified Taylor-Couette. Withjack and Chen (1974) and later Boubnov et al. (1995) experimentally found, that non-axisymmetric instabilities exist in axially saltwater-stratified Taylor-Couette flows even beyond the Rayleigh limit. Le Gal and Le Bars (2007) confirmed the linear stability analysis by Shalybkov and Rüdiger (2005) with respect to the course of the critical curve in a diagram spanned by the Reynolds number $Re = \Omega_{in}r_{in}(r_{out}-r_{in})/\nu$ and the angular velocity ratio μ. Azimuthal wavenumbers $m > 1$ cross the Rayleigh line and approach asymptotically the quasi-galactic line $\mu = \eta$, but wavenumber $m = 0$ (e.g. classical Taylor vortices) never crosses the Rayleigh limit. In a resent paper, Ibanez et al. (2016) reported that the stability criterion $\mu = \eta$, proposed by Shalybkov and Rüdiger (2005) is violated for buoyancy frequencies sufficiently large.

First experiments with a water filled Taylor-Couette tank cooled from below and heated from above have been conducted by Wu (2013) at the department of Aerodynamics and Fluidmechanics BTU CS. He found the line of marginal instability, separating stable from unstable flow for Reynolds numbers $Re \in [1000, 2000]$ and Froude number $Fr = \Omega_{in}/N \approx 1.8$. The Froude number is the normalized rotation rate, being $N^2 = \alpha g\Delta T/\Delta z$ the buoyancy frequency, where α is the coefficient of thermal expansion, g the gravity of the Earth and $\Delta T/\Delta z$ the axial temperature gradient. An additionally study of Stapelfeld (2015) investigated the flow with silicone oil for $Re < 10^3$ and $Fr = 2$. In accordance with linear theory they found that for $Re < 800$ the critical curve approaches the line $\mu = \eta = 0.517$. However, for larger Re the curve bends backwards to smaller μ and approaches a line in between the Rayleigh line and the line $\mu = \eta$. This backward bending is consistent with recent linear stability computations from Gellert and Rüdiger (2016). From this new findings it appears that the transition curves are more complicated as assumed e.g. in Le Bars and Le Gal (2007).

Wu (2013) and Stapelfeld (2015) used just visualization techniques to identify the line of marginal instability. In order to quantify the region and the phenomenon of the SRI we perform measurements of velocity fields with Particle Image Velocimetry (PIV). A remote controlled, height-adjustable and co-rotating mini-PIV system that supports two lasers has been used. The two lasers give us the opportunity to measure simultaneously velocities in a radial-azimuthal and a radial-axial plane. The complex optical accessibility due to the curved outer cylinder is described in detail. We present exemplary results and compare those with the axially invariant Taylor-Couette solution for the angular velocity.

Karlsruhe, Germany, ISBN 978-3-9816764-2-6

Experimental methods

Experiments were conducted in a modified Taylor-Couette tank (figure 1, left). Its height is h = 700 mm with inner radius r_{in} = 75 mm and outer radius r_{out} = 145 mm. The governing geometrical parameters are the radius ratio $\eta = 0.5172$ and aspect ratio $\Gamma = h/(r_{out} - r_{in}) = 10$. The outer cylinder is made of acrylic glass and it is accessible for Particle Image Velocimetry (PIV) (Adrian and Westerweel. 2010). The inner cylinder is made of aluminum and is anodized in order to suppress parasitic optical reflection. Both horizontal end-plates are connected to the outer cylinder. Contrary to experiments with axial stable salt-stratification (Thorpe 1966, Withjack and Chen. 1974, Boubnov et al. 2007, Le Bar and Le Gal. 2007) we use a temperature-stratified fluid. The experiment is heated from above and cooled from below. On the upper end-plate twelve Peltier elements (type TEC263) have been installed. Six of them operate as heat source and were mounted in hexagonal order at the inner part of the plate. All further Peltier elements work as cooling system. They are mounted on top of aluminum blocks. Water is cooled inside the aluminum blocks and continuously pumped downward into a reservoir mounted below the bottom aluminum end-plate. The temperature difference between top and bottom is adjustable in a range of about 1 − 5 K. Note that for efficient cooling the elements need an extra passive cooling that is realized by fans. The inner and outer cylinder is driven independently by two DC motor units. The motor units are controlled by servo amplifiers.

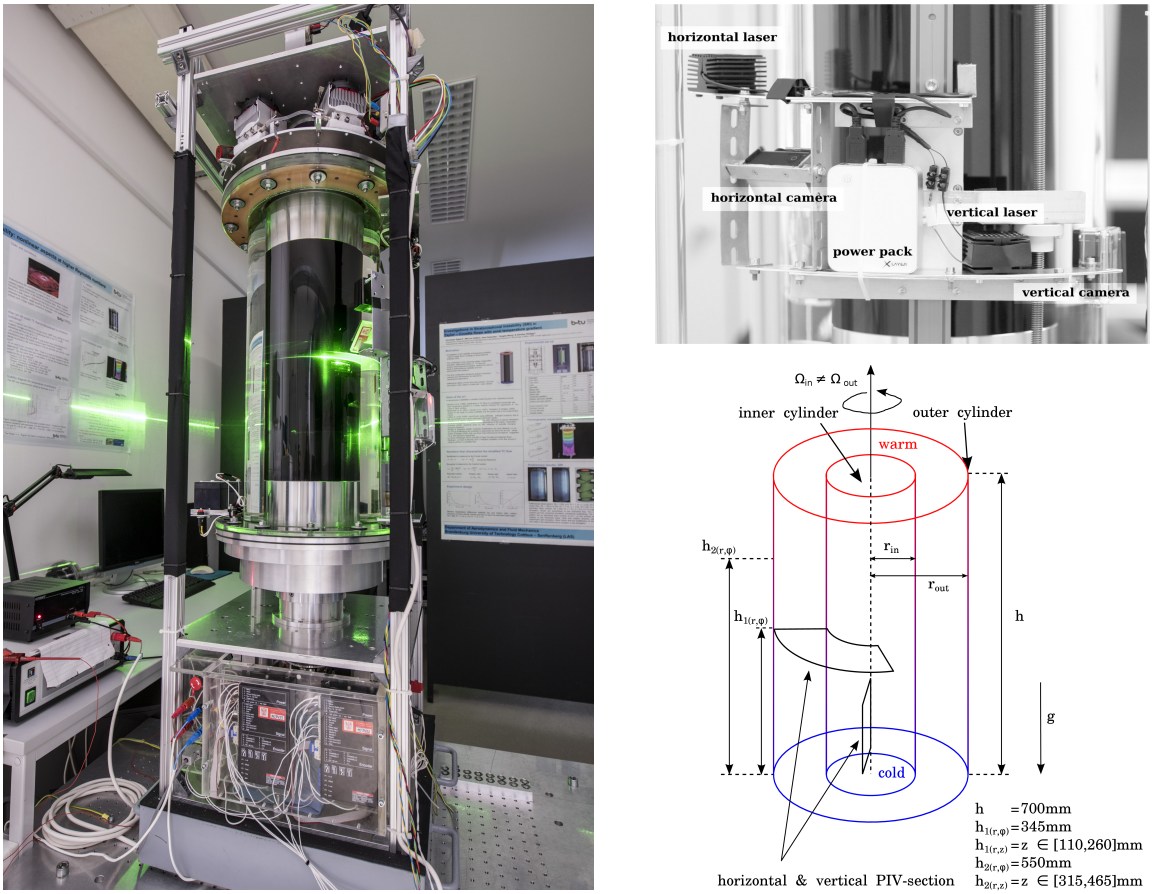

Figure 1: Left The SRI experiment at BTU Cottbus – Senftenberg. Right: Co-rotating mini-PIV system (top) and definition of the geometrical parameters and the orientation of the laser sheets (bottom).

We adjust the rotation rate of the inner cylinder in the range of $0.19 \pm 0.0038 < \Omega_{in} < 2.381 \pm 0.0476$ rad/s to achieve the desired Reynolds numbers $Re \in [200, 2500]$. Variation of μ is achieved by changing the rotation rate Ω_{out} of the outer cylinder. The tank is filled with silicone

oil M5. Physical parameters are listed in table 1. All experiments start by setting the appropriate temperature gradient. To achieve a nearly linear axial temperature stratification to start with - and hence a constant buoyancy frequency - the fluid is mixed by rotating the inner cylinder rather fast while keeping the outer cylinder at rest. The process needs to be repeated several times. It requires approximately 4−6 hours to achieve a linear temperature gradient of 2 − 4 K. Temperature is measured with five thermocouples (type AD590) connected to each end-plate. Additionally, the vertical profile is analyzed with an infrared camera (type IR-TCM 640hr, resolution 640×480 px). After reaching a linear stratification, we wait another 20 minutes to guarantee that the fluid inside the Taylor-Couette tank is at rest. The viscous decay rate is given by $\tau_\nu = \Omega^{-1}\,Ek^{-1/2}$ (Greenspan and Howard. 1963), being $Ek = \nu/(\Omega H^2)$ the Ekman number, Ω the rotation frequency of the inner cylinder and H the height of the tank. Substituting our parameters into these equations yields a viscous decay time of approximately 4 minutes, well below the time we used for the spin-down.
Each experiment start with the fluid at rest. We set the rotation rate of the outer cylinder first followed by setting the rotation rate of the inner cylinder. Achieving the desired tuple (Re,μ), we wait another 20 minutes to guarantee decay/saturation of the SRI. After an experiment is completed and the instability is damped out, we check the temperature gradient and the linearity of the stratification and a new experiment can be started.

density	ρ	923 kg/m^3
kinematic viscosity	ν	$5\cdot10^{-6}$ m^2/s
coefficient of thermal expansion	α (0…150 °C)	$1.08\cdot10^{-3}$ 1/K
thermal conductivity	κ	0.133 W/Km
specific heat	c_p	1630 J/kgK
Prandtl number	Pr	56.56
Earth's gravity	g	9.81 m/s^2

Table 1: Physical properties of silicone oil M5 (at 25°C)

Measurement technique

We measure the flow with a co-rotating mini-PIV system (figure 1, right). A continuous green (532 nm) laser module with line generator mounted on a cross beam produces a 2 mm thick horizontal (r,φ) laser sheet. A ’GoPro Hero 4 black edition’ camera with a tilted viewing angle of approximately 45° is mounted below the laser sheet. Using a ’medium’ field of view (FOV) we observe more than a sixth of the full horizontal circular section (φ ≈ 65°). A second green laser module with line generator producing again a 2mm thick vertical laser sheet is also mounted on the cross beam. A second 'GoPro Hero 4 black edition' camera records the flow with a tilted viewing angle. Both cameras enable wireless synchronized high-resolution recordings with a resolution of 1080×1920 px and a frame rate of 24/30 fps. The cross beam is mounted on a remote controlled and height adjustable traverse. This enables us to adjust the measurement height during operation. The recording time is approximately 15 minutes.

Calibration and post-processing

We calibrated the FOV's with chess board patterns (see exemplary figure 2, left). From each record we extract gray scale images using a command line tool to convert multimedia files between formats called 'ffmpeg'. The distortions appearing due to the curvature of the outer cylinder, the camera's fish-eye lens effect, the perspective view and optical reflections we correct by applying a 'Polynomial' distortion method. The polynomial distortion maps pairs of

source control points (X_S,Y_S) to destination control points (X_D,Y_D) using a standard polynomial equation of order five. The method uses all the control point pairs given to calculate the appropriate coefficients (C_{iX},C_{iY}), being i = 0,…,21,

$$X_D = C_{21X}X_S^5 + C_{20X}Y_S^5 + \ldots + C_{3X}X_SY_S + C_{2X}X_S + C_{1X}Y_S + C_{0X},$$
$$Y_D = C_{21Y}X_S^5 + C_{20Y}Y_S^5 + \ldots + C_{3Y}X_SY_S + C_{2Y}X_S + C_{1Y}Y_S + C_{0Y}.$$

For efficiency we use the library 'convert' of 'ImageMagick's' software package and *parallelized* the code. Additionally, we determined the origin of the segment needed for polar coordinate transformations (figure 2, solid line). The velocity is analyzed using a *parallelized* version of MatPIV (Sveen 2004) with an interrogation window size of 32×32 px and an overlap of 50%, resulting in a spatial resolution of approximately 1.6 mm. The particle displacement error is 0.1 pixel (Nobach and Bodenschatz. 2009) that implies by additional use of a moving average (window size 25 vector fields) an absolute error ε in velocity of 0.048 mm/s (ε ≤ 4.8% with respect to v_r and $\Delta v_\varphi = \overline{v}^t_\varphi - v_\varphi(t)$).
Note, in the following discussion we focus on the horizontal section (level $h_1(r,\varphi)$ figure 1, bottom right) only.

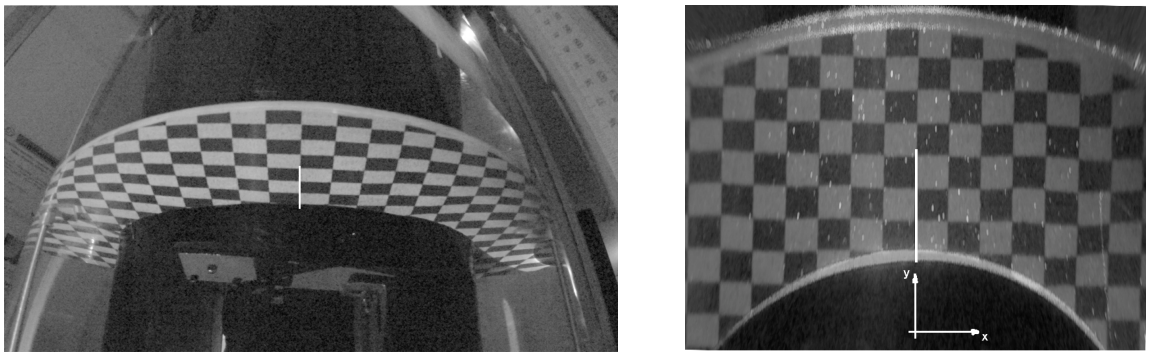

Figure 2: Left: Distorted FOV due to curvature of the cylinder, camera's fish-eye lens effect, perspective view and optical reflections. Right: Composite of undistorted chess board pattern and raw PIV data. The solid line represents the origin y = 0 mm.

Results

We measured several axial symmetric flows. A good test of the accuracy of our PIV system is a comparison between the time-averaged azimuthal velocity profile and the axially invariant Taylor-Couette solution. Leclercq et al. (2016) showed numerically that linear axial stratifica-

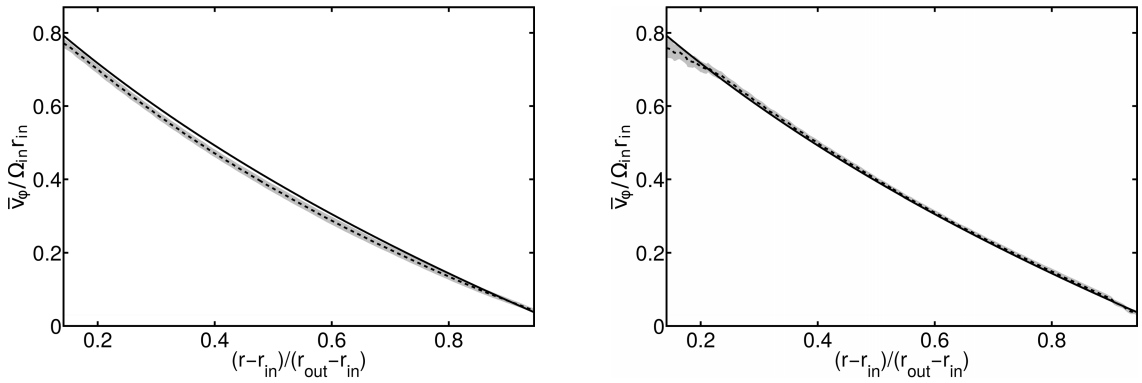

Figure 3: Comparison of the axially invariant Taylor-Couette solution (solid line) and time-averaged azimuthal velocity profile (dashed line). The standard deviation of the profiles is shown as shaded area. Left: Re = 600, μ = 0.502. Right: Re = 800, μ = 0.450.

tion or partially strong stratification at the end-plates (see their figure 7 and 11) can reduce the unwished Ekman effects. Hence we expect a good match between the axially invariant Taylor-Couette solution and the measurements. Indeed, we find an almost perfect match between the time-averaged azimuthal flow and the theoretical Taylor-Couette solution. Figure 3 (left) shows exemplary a result for Re = 600, μ = 0.502. An almost perfect match is visible. The profile measured (dashed line) is slightly smaller than the theoretical profile (solid line) and confirms the finding of Leclercq et al. (2016). Still there are small azimuthal flow perturbations due to geometrical deviations of the outer cylinder, shown as shaded area (standard deviation of time-averaged azimuthal velocity). Figure 3 (right) confirms this finding for Re = 800, μ = 0.450 (right). Again both profiles match almost perfect. Largest deviations are visible in the vicinity of the inner cylinder and may be explained by strong reflections of laser light and still remaining small boundary layer effects at the end-plates (Avila et al. 2008).

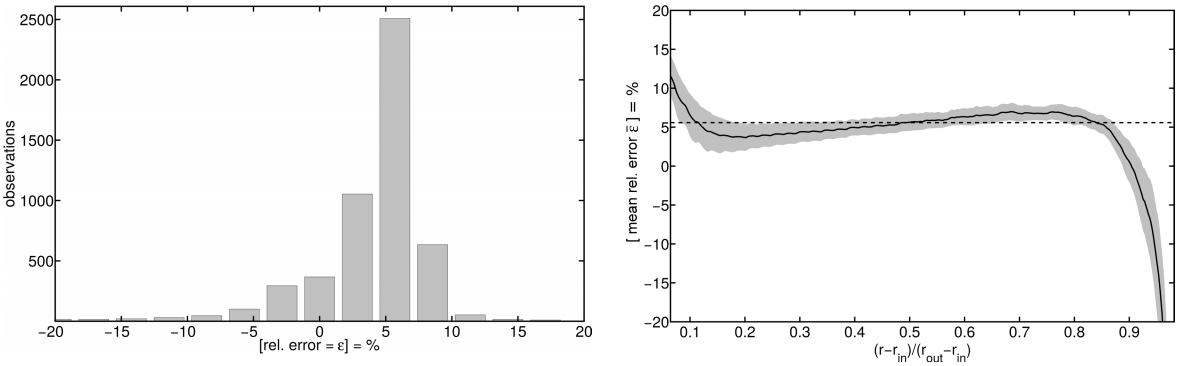

Figure 4: Left: Graphical representation of the distribution of the relative error $[\varepsilon(r) = (v_{TC} - \bar{v}_\varphi)/v_{TC}]$ = % of data for all stable cases. The elements in ε are sorted into 45 equally spaced bins. The most observations can be found centered around ε being approximately 5%. Right: Arithmetic average $\bar{\varepsilon}(r)$ (solid line) and standard deviation $\sigma(r)$ (shaded area) computed from all stable flows. The dashed line indicates the weighted arithmetic mean of the relative error.

Next, we focus on the relative error $\varepsilon(r) = (v_{TC} - \bar{v}_\varphi)/v_{TC}$. We measured nine stable flows at different Reynolds numbers. The relative errors are sorted into 45 equally spaced bins and presented as histogram (figure 4, left). A relative error of about 5% is most frequently observed. The number of observations decrease rapidly with increasing/decreasing relative error. To substantiate the finding, we compute the arithmetic average of the relative error $\bar{\varepsilon}(r)$ (solid line, figure 4 right) and its standard deviation $\sigma(r)$ (shaded area, figure 4 right). As the radial coordinate approaches one (radius r_{out}), the normalized Taylor-Couette solution approaches zero, causing ε goes to infinity. Therefore, the averaged relative error is not well represented in the vicinity to the outer cylinder. A more robust result can be found by examining the weighted arithmetic mean of the relative error

$$\bar{\varepsilon} = \frac{\sum_i w_i \varepsilon(r_i)}{\sum_i w_i} ,$$

with weights $w_i = \sigma(r_i)^{-2}$. We computed its value to be $\bar{\varepsilon}$ = 5.58% (dashed line, figure 4 right). The standard deviation of the weighted mean relative error is,

$$\sigma_{\bar{\varepsilon}} = \frac{1}{\sum_i \sigma(r_i)^{-2}}$$

and found to be $\sigma_{\bar{\varepsilon}}$ = 0.052%.

Karlsruhe, Germany, ISBN 978-3-9816764-2-6

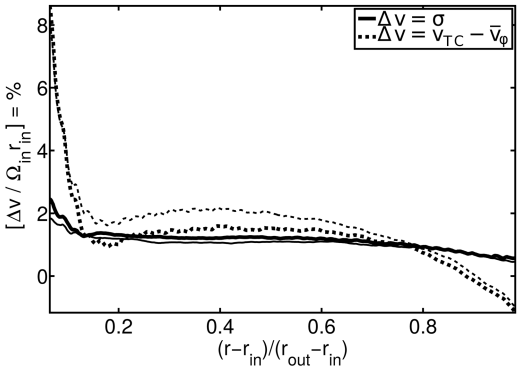

Figure 5: Comparison of the absolute error $\Delta v/\Omega_{in}r_{in}$. We chose data of stable flows Re = 400, μ = 0.492 (thick solid and dashed line) and Re = 600, μ = 0.502 (thin solid and dashed line). Solid lines represent the standard deviation of the time-averaged azimuthal velocity. Dashed lines belong to the deviation of the axially invariant Taylor-Couette solution and the time-averaged azimuthal velocity profile.

A comparison of the absolute error $\Delta v/\Omega_{in}r_{in}$ concludes the study, being Δv the standard deviation σ of the time-averaged azimuthal velocity or the difference of the Taylor-Couette solution regarding the time-averaged azimuthal velocity. Figure 5 shows exemplary absolute errors. We chose data of stable flows Re = 400, μ = 0.492 (thick solid and dashed line) and Re = 600, μ = 0.502 (thin solid and dashed line). The absolute error is approximately 1-2% in the bulk and becomes larger towards the rigid boundaries of the inner and outer cylinder. Larger errors at the inner cylinder can be devoted to strong laser-light reflections. The standard deviation reflects small perturbations caused due to deviations of the outer cylinder. Basically, there is a tiny precession of the outer cylinder that forces an inertial mode with frequency of the outer cylinder. Especially for Re = 400 we find the standard deviation of the perturbation of the same size than the difference $v_{TC} - \bar{v}_{\varphi}$.

Conclusion

PIV errors in a Taylor-Couette tank with axial stratification have been studied. Top and bottom end-plates are not accessible for quantitative measurement techniques, e.g. Laser Doppler Anemometry or PIV. Therefore we built a co-rotating, remote controlled and height adjustable mini-PIV system supporting a horizontal and vertical laser and two cameras. The FOVs are distorted due to the curvature of the outer cylinder, the camera's fish-eye lens effect, the perspective view of the cameras and optical reflections. We calibrated the FOV's and corrected distortions by applying a 'Polynomial' distortion method. We estimated the accuracy of the measurement technique by comparing the axially invariant Taylor-Couette solution together with time-averaged azimuthal velocity profiles. We showed for the first time experimentally the reduction of global end-wall effects in a linear stratified Taylor-Couette flow and hence experimentally confirm the numerical findings of Leclercq (2016). We estimated the absolute error of the mini-PIV system to be approximately 2% and the relative error to be 5.58% ± 0.052%. This shows that the well known PIV measurement technique together with the applied novel calibration technique is suitable to quantify Taylor-Couette flows and the SRI.

Acknowledgement

This work is part of the project ‘Drehimpulstransport in einem geschichteten Taylor-Couette Experiment mit Anwendungen auf Akkretionsscheiben’, financed by the German Science Foundation (DFG). The authors wish to thank Ludwig Stapelfeld and Vilko Ruoff for technical assistance.

References

Adrian, R. J. and Westerweel, J., 2010: “Particle Image Velocimetry”, Cambridge University Press
Avila, M., Grimes, M., Lopez, J. M., Marques, F., 2008: “Global endwall effects on centrifugally stable flows”, Phys. Fluids 20, 104104
Boubnov, B. M., Gledzer, E. B., Hopfinger, E. J., 2007: “Stratified circular Couette flow: instability and flow regimes”, JFM 292, pp. 333-358
Gellert, M., Rüdiger, G., 2009: “Stratorotational instability in Taylor-Couette flow heated from above”, JFM 623, pp. 375-385
Greenspan, H. P., Howard, L. N., 1963: “On a time-dependent motion of a rotating fluid”, JFM 17, pp. 385-404
Ibanez, R., Swinney, H. L., Rodenborn, B., 2016: “Observations of the stratorotational instability in rotating concentric cylinders”, arXiv 1604.02963v1 [physics.flu-dyn], 11 Apr 2016
Le Bars, M. and Le Gal, P., 2007: “Experimental analysis of the stratorotational instability in a cylindrical Couette flow”, Phys. Rev. Lett., Vol. 99, 064502.
Leclercq, C., Patridge, J. L., Augier, P., Dalziel, S., Kerswell, R. R., 2016: “Using stratification to mitigate end effects in quasi-Keplerian Taylor-Couette flow”, JFM 791, pp. 608-630.
Nobach, H. and Bodenschatz, E., 2009: “Limitations of accuracy in PIV due to individual variations of particle image intensities”, Exp. Fluids 47, pp. 27-38
Rüdiger, G., Hollerbach, R., Kitchatinov, L. L., 2013: “Magnetic Processes in Astrophysics” Wiley-VCH.
Rüdiger, G. and Gellert, M., 2016: personal communication
Shalybkov, D. and Rüdiger, G., 2005: “Stability of density-stratified viscous Taylor-Couette flows”, Astron. Astrophys., Vol. 438, pp. 411ff.
Stapelfeld, L., 2015: “Experiments on 'stratorotational instability' with thermal stratification”, Diploma thesis, BTU Cottbus - Senftenberg
Sveen, J. K., 2004: “An introduction to MatPIV v. 1.6.1”, eprint series, Dept. of Math. University of Oslo, Mechanics and Applied Mathematics, No. 2, ISSN 0809-4403
Thorpe, S. A., 1966: “Notes on 1966 Summer Geophysical Fluid Dynamics”, Woods Hole Oceanographic Institute, Woods Hole, MA, p. 80
Withjack, E. M. and Chen, C. F., 1974: “An experimental study of Couette instability of stratified fluids”, JFM 66, pp. 725-737
Wu, B., 2013: “Experimental study of the transition to stratorotational instability”, Master thesis, BTU Cottbus - Senftenberg